Large-amplitude Q_n-Q_p collectivity in the neutron-rich oxygen isotope ^{20}O

A. P. Severyukhin,[1] M. Bender,[2,3] H. Flocard,[4] and P.-H. Heenen[5]
[1]*Bogoliubov Laboratory of Theoretical Physics, Joint Institute for Nuclear Research, RU-141980 Dubna, Moscow region, Russia*
[2]*Dapnia/SPhN, CEA Saclay, F-91191 Gif sur Yvette Cedex, France*
[3]*Université Bordeaux 1; CNRS/IN2P3; Centre d'Etudes Nucléaires de Bordeaux Gradignan, UMR5797, Chemin du Solarium, BP120, F-33175 Gradignan, France*
[4]*CNRS-IN2P3, Université Paris XI, CSNSM, Bt. 104, F-91405 Orsay Campus, France*
[5]*PNTPM, CP229, Université Libre de Bruxelles, B-1050 Brussels, Belgium*
(Received 12 January 2007; published 4 June 2007)

By means of HFB calculations with independent constraints on axial neutron and proton quadrupole moments $\hat{Q}_n$ and $\hat{Q}_p$, we investigate the large amplitude isoscalar and isovector deformation properties of the neutron-rich isotope ^{20}O. Using the particle-number and angular-momentum projected generator coordinate method, we analyze the collective dynamics in the $\{\langle\hat{Q}_n\rangle, \langle\hat{Q}_p\rangle\}$ plane. The parametrization SLy4 of the Skyrme interaction is used for all calculations in connection with a density-dependent zero-range pairing interaction. Our results show that already for this moderately neutron-rich nucleus the transition moments are modified when independent neutron and proton collective dynamics are allowed.

DOI: 10.1103/PhysRevC.75.064303 PACS number(s): 21.60.Jz, 21.10.Gv, 21.10.Ky, 27.30.+t

I. INTRODUCTION

The dominance of the neutron-proton attraction is one of the main characteristics of the effective nucleon-nucleon interaction. It can be traced back to the isospin symmetry of the nucleon-nucleon force and to the cooperation of its $T = 0$ and $T = 1$ channels. As a result, isovector collective modes have a much higher excitation energy than their isoscalar counterparts. On the other hand, the study of nuclei away from the stability line have challenged some of the standard nuclear structure concepts. In particular, the discovery of extended neutron halos in some neutron-rich nuclei has been, at least partly, attributed to a decoupling of the two nucleonic distributions when N is much larger than Z. Other interesting phenomena such as pygmy resonances have been observed, which are clear indications that the excitation of isovector modes is easier in neutron-rich isotopes than in stable ones. The pygmy modes are associated with dipolar excitations involving a restricted number of nucleons and, partly for this reason, carry a small fraction of the sum rule only. On the other hand, most of the low-energy collective structure remains dominated by isoscalar large amplitude quadrupole dynamics, leading in many regions of the nuclear chart to static ground-state deformation.

The strong proton shell closure at $Z = 8$ and the already good experimental knowledge of the chain of oxygen isotopes from ^{16}O up to the drip line at ^{24}O [1–18] makes oxygen an attractive element for a first investigation. In fact, the experimental effort for these isotopes has spurred a number of theoretical studies, either based on the mean-field method [13,19–24], or on the shell model [18,25–27]. Within the framework of mean-field approaches, all investigations of collective dynamics have up to now exclusively studied excitations around the mean-field ground-state configuration, which always corresponds to a spherical shape. An important result from both experimental and theoretical work is the weakening of the $N = 20$ shell effect (both ^{26}O and ^{28}O are not bound [3–6]) along with evidences for a local subshell predicted at either $N = 14$ [13] or $N = 16$ [23].

For these reasons, we have chosen to investigate the effect of a large neutron excess on both isoscalar and isovector quadrupole modes of the oxygen isotopes in a consistent manner. This first article presents our method and gives an illustration for the nucleus ^{20}O. In order to treat small- and large-amplitude collective motion on the same footing, we perform our analysis within the framework of the projected generator coordinate method (GCM) [28–30] based on Hartree-Fock-Bogoliubov (HFB) wave functions. A consistent simultaneous treatment of isovector and isoscalar dynamics is obtained by working in a collective space in which neutron and proton deformations are allowed to vary independently.

II. DEFINITION OF THE COLLECTIVE SPACE

Let us briefly summarize the different steps involved in our method (see Refs. [28–30] for more details).

In the GCM, the collective dynamics is constrained by the choice of a variational space, the so-called collective space. For the present study, this space is generated by a nonorthogonal basis of particle-number and angular-momentum projected HFB states.

A. Constrained HFB

The HFB states are obtained from self-consistent calculations using either a single constraint on the axial mass quadrupole moment, or a double constraint acting separately on the axial neutron and proton quadrupole moments

$$\hat{Q} = 2\hat{z}^2 - \hat{x}^2 - \hat{y}^2. \tag{1}$$

The resulting HFB states are denoted $|q\rangle$, where q labels the collective variables. In the case of a single constraint, q is

identified with the expectation value $\langle\hat{Q}_t\rangle$ of the total (mass) quadrupole moment. In this case, the relative contributions of the neutron and proton quadrupole moment, $\langle\hat{Q}_n\rangle$ and $\langle\hat{Q}_p\rangle$, to the total quadrupole moment $\langle\hat{Q}_t\rangle$ are entirely determined by the CHFB minimization process. In the case of double constraint, the proton $\langle\hat{Q}_p\rangle$ and neutron $\langle\hat{Q}_n\rangle$ quadrupole moments are taken as independent constraints, and the collective variable q becomes two-dimensional, $q = \{\langle\hat{Q}_n\rangle, \langle\hat{Q}_p\rangle\}$.

As in our previous studies [28–30], the Lipkin-Nogami (LN) prescription is used to avoid a spurious collapse of pairing correlations in the HFB wave functions for some values of the quadrupole moment. The HFB-LN equations are solved with the two-basis method described in Ref. [31]. The HFB states are chosen to be time-reversal invariant, and the single-particle states are eigenstates of parity, z signature, and projection of isospin as in Ref. [32]. They are represented on 1/8 of a cubic mesh of size 11.6 fm with a distance of 0.8 fm between mesh points.

We use the effective Skyrme interaction SLy4 in the particle-hole channel [33] together with a surface-peaked density-dependent zero-range force acting in the particle-particle (pairing) channel. Its strength is taken equal to -1000 MeV fm^3 in connection with two soft cutoffs at 5 MeV above and below the Fermi energies as introduced in Ref. [34].

As a matter of fact, the contribution of the quadrupole constraint to the one-body potentials has a numerically pathological behavior at large distances. Indeed, depending on whether the deformation is prolate or oblate, the constraining field decreases as $-r^2$ along the z axis or in the perpendicular plane, respectively. When solving the mean-field equations on a mesh in coordinate space, the finite size of the mesh cuts the constraint at large distances, but there always remain attractive pockets at the boundaries of the box, which will either distort the single-particle states around the continuum threshold, or even bind them.[1] As soon as these states have a sizable occupation, as it may happen in neutron-rich systems, the constraint might lead to spurious contributions to the density outside of the nucleus. The large box size that has to be chosen in neutron-rich systems even amplifies the problem; hence, the constraint has to be damped at large distances from the nucleus. We achieve this by multiplying the constraining operator with a Fermi function as proposed in Ref. [36]. We first define an equidensity surface on which the nucleon density ρ is equal to one tenth of the maximal density $\rho_{\max}$. The cutoff takes place smoothly over a width equal to a for radii exceeding the surface by a distance δr_c.

The parameters δr_c and a have to be selected such that they do not affect the results over the range of considered deformations. The main role is played by the cutoff distance δr_c which we have set to 5.5 fm, slightly larger than the recommended value of Ref. [36], while the width parameter was set to $a = 0.4$ fm.

[1]When the CHFB calculations are performed by expanding single-particle orbitals on a basis such as an oscillator basis, the effective cutoff is provided by the long-range behavior of the basis wave functions.

B. Particle-number and angular-momentum projected GCM

The second step of our method is the construction of the collective basis

$$|JMq\rangle = \frac{1}{\mathcal{N}_{J,q}}\hat{P}^J_{M0}\hat{P}^N\hat{P}^Z|q\rangle, \tag{2}$$

by means of projection operators, where $\mathcal{N}_{J,q} = \langle q|\hat{P}^J_{00}\hat{P}^N\hat{P}^Z|q\rangle^{1/2}$ is a normalization factor. Although the particle numbers of the intrinsic and projected states might be chosen different, the mean-field states have always been constrained to have $N = 12$ and $Z = 8$ as the expectation value of the neutron and proton numbers. For the sake of simple notation. we drop the particle number indices for the rest of the paper.

The operator $\hat{P}^J_{\mathrm{MK}}$ restores the rotational symmetry broken by the intrinsic deformation of the nucleus and provides a many-body state with good total angular momentum J and projection M on one axis in the laboratory frame of reference. As we consider axial deformation with the z axis as symmetry axis only, the projection of the intrinsic angular momentum on this axis K is always equal to zero by construction. We limit our study to values of the total angular momentum J equal to zero and two.

In the next stage, we construct collective wave functions from a linear combination of projected states

$$|JMk\rangle = \sum_q f^J_{kq}|JMq\rangle. \tag{3}$$

The weights $f^J_{k,q}$ of the projected HFB states are determined from the minimization of the total energy

$$E^J_k = \frac{\langle JMk|\hat{H}|JMk\rangle}{\langle JMk|JMk\rangle}. \tag{4}$$

For each angular momentum J, the index k labels the solutions of the minimization procedure. The variation of the energy ($\delta_f E^J_k = 0$) leads to the Hill-Wheeler-Griffin equation

$$\sum_{q'}\left(\mathcal{H}^J_{qq'} - E^J_k\mathcal{I}^J_{qq'}\right)f^J_{kq'} = 0. \tag{5}$$

Its solution requires to compute the off-diagonal matrix elements of the energy and overlap kernels

$$\mathcal{H}^J_{qq'} = \langle JMq|\hat{H}|JMq'\rangle, \tag{6}$$

$$\mathcal{I}^J_{qq'} = \langle JMq|JMq'\rangle, \tag{7}$$

which are evaluated with the techniques described in [28]. The calculation of electromagnetic $E2$ transitions requires the additional evaluation of the projected GCM kernels associated with the electric quadrupole tensor operators $\hat{Q}_{2\mu}$, see the appendix of Ref. [34].

Two further comments are in order. First, the angular-momentum projection provides a transformation from the intrinsic to the laboratory frame of reference. As a consequence,

every state $|J = 0M = 0q\rangle$ is *spherical* in the laboratory frame of reference irrespective of the intrinsic quadrupole deformation associated with the collective variable q. Second, the weights f^J_{kq} are connected to the set of orthogonal collective wave functions g^J_{kq} through [37]

$$g^J_{kq} = \sum_{q'} (\mathcal{I}^J)^{1/2}_{qq'} f^J_{kq}, \tag{8}$$

where $(\mathcal{I}^J)^{1/2}$ represents the kernel whose square convolution gives $\mathcal{I}^J$.

Given the number of grid points selected on the $\{\langle\hat{Q}_n\rangle, \langle\hat{Q}_p\rangle\}$ surface (about 25), the number of gauge angles to restore the particle numbers (seven for both protons and neutrons) and the number of Euler required for an accurate angular-momentum projection (12), each calculation corresponds to the mixing of about 15000 N-body wave functions. By construction, the basis of projected HFB states $|JMq\rangle$ is not orthogonal (separately for each value of J and M). Using too many states $|JMq\rangle$ in a GCM calculation might lead to an overcomplete basis that generates many near-zero eigenvalues of the overlap kernel $\mathcal{I}_{qq'}$, which might lead to spurious states. This difficulty is treated with the techniques described in Refs. [28–30].

III. RESULTS

In the left panel of Fig. 1, we show the CHFB energy curve obtained with a single constraint on the mass quadrupole deformation as a function of the dimensionless quadrupole deformation $\beta_{2,t}$

$$\beta_{2,t} = \sqrt{\frac{5}{16\pi}} \frac{4\pi Q_t}{3R^2 A}, \tag{9}$$

where the radius constant is given by $R = 1.2A^{1/3}$ fm. In light nuclei and at large deformation, the values of the β_2 as defined through Eq. (9) might be much larger than the multipole deformation parameters in a liquid drop model. As in our previous publications, the mean-field energy curves that are presented are already particle-number projected to avoid the ambiguities related to the Lipkin-Nogami correction to the mean-field energy. In the right panel of Fig. 1, we show the path followed by the single-constraint calculation in the two-dimensional plane of proton and neutron deformations

$$\beta_{2,n} = \sqrt{\frac{5}{16\pi}} \frac{4\pi Q_n}{3R^2 N}, \tag{10a}$$

$$\beta_{2,p} = \sqrt{\frac{5}{16\pi}} \frac{4\pi Q_p}{3R^2 Z}. \tag{10b}$$

For a given total quadrupole deformation, $\beta_{2,n}$ and $\beta_{2,p}$ take the values that minimize the total energy. Thus, this path corresponds to the valley that is obtained in a double-constraint calculation. As long as the radii of the proton and neutron density distributions are not too different, the use of $\beta_{2,n}$ and $\beta_{2,p}$ removes most of the trivial scaling of the neutron and proton quadrupole moments associated with different values of N and Z. With such coordinates, equal neutron and proton deformations of a saturating system where the neutron density is strictly proportional to the proton density would lie on the first bisector, represented by the dotted line in the right panel of Fig. 1. Already for not too large deformations, the path diverts from the line of equal proton and neutron deformations, indicating that for both prolate and oblate shapes the neutrons are always more deformed than the protons.

The Nilsson diagrams of neutron and proton single-particle energies as obtained with SLy4 for ^{20}O are shown in Fig. 2 for states along the path of Fig. 1. For the neutrons, the upward shift of the Fermi energy leads to a particle-hole (ph) excitation at $\beta_{2,t} \approx 1.8$ ($\langle\hat{Q}_t\rangle \approx 300$ fm^2) in which the ν $p_{1/2}$ level is exchanged with the ν $f_{7/2}$ $m = 1/2$ level. The sequence of

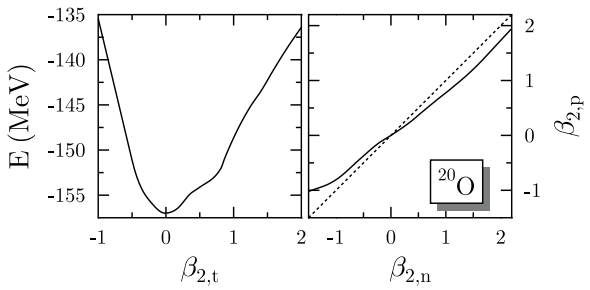

FIG. 1. Particle-number projected energy curve obtained with a single constraint on the mass quadrupole moment (left) and the corresponding path in the plane of proton and neutron quadrupole deformation (right). The dotted line in the right panel corresponds to the line of equal proton and neutron deformation $\beta_{2,n} = \beta_{2,p}$.

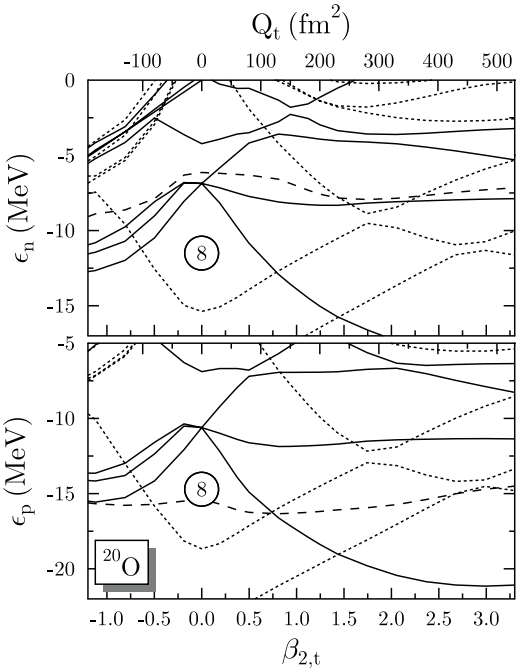

FIG. 2. Neutron (top) and proton (bottom) single-particle energies (in MeV) versus mass quadrupole deformation (bottom horizontal scales) and mass quadrupole moment (top horizontal scale). Solid (dotted) lines correspond to positive (negative) parity states. The dashed lines represent the Fermi energies of protons and neutrons, respectively.

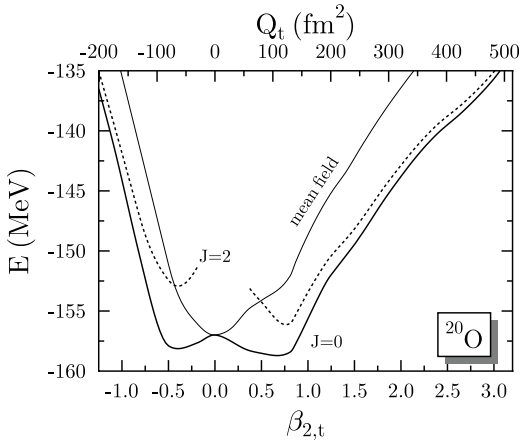

FIG. 3. Particle-number projected mean-field (solid curve) and particle-number and angular-momentum projected deformation energy curves of ^{20}O as a function of the mass quadrupole deformation.

crossings at the Fermi surface for the protons corresponds to a 2p-2h ($\beta \approx 0.6$) and 4p-4h proton excitation ($\beta \approx 3$) and is close to that obtained for ^{16}O in Ref. [35].

The deformation energy curves corresponding to three different calculations are drawn in Fig. 3. The number-projected HFB energy curves are represented by a thin solid curve. It displays a pattern typical for an oxygen isotope: a well-defined spherical minimum and a steep rise of the energy versus deformation, with a shoulder hinted at moderate prolate deformation. For the energy curve projected on $J = 0$, the behavior is markedly different. The energy does not vary much over the range $-0.5 < \beta_{2,t} < 0.8$, or $-100\,\mathrm{fm}^2 < \langle \hat{Q}_t \rangle < 200\,\mathrm{fm}^2$, equivalently. This reflects that the 0p-0h configuration with respect to the spherical HFB solution is the dominant component of the $J = 0$ wave function and that this component is present in the mean-field wave function over a rather large range of deformations. The configurations with a deformation $\beta_{2,t}$ beyond 0.8, or $\langle \hat{Q}_t \rangle \simeq 120\ \mathrm{fm}^2$ can be associated with 2p-2h proton excitations across the magic gap at $Z = 8$. By contrast, the 2^+ energy curve displays pronounced minima. The finding that for almost all deformations but those close to sphericity the number projected CHFB curve lies significantly above the 0^+ and 2^+ curves demonstrates that components of higher angular momentum have a non-negligible amplitude in the intrinsic HFB states $|q\rangle$.

For the rest of this work, we consider only such neutron and proton deformations, that the HFB excitation energy does not exceed 20 MeV. The associated zone in the $\{\langle \hat{Q}_n \rangle, \langle \hat{Q}_p \rangle\}$ plane corresponds to configurations in which the proton $1s_{1/2^+}$ and $1p_{3/2^-}$ orbitals remain filled. In Fig. 4 we show the $J = 0$ (top) and $J = 2$ (bottom) projected energy surfaces. The $J = 0$ surface displays two minima, in the quadrants where both neutrons and protons have either prolate or oblate deformations. One notes that the energy rises slowly along the axis $\langle \hat{Q}_n \rangle = 0$ in contrast to the single constraint path indicated by the dashed line. A similar, although less marked tendency exists along the $\langle \hat{Q}_p \rangle = 0$ axis. This indicates that on the one hand the 0^+ component in the intrinsic HFB state is mostly unchanged along these axes and that on the other hand there

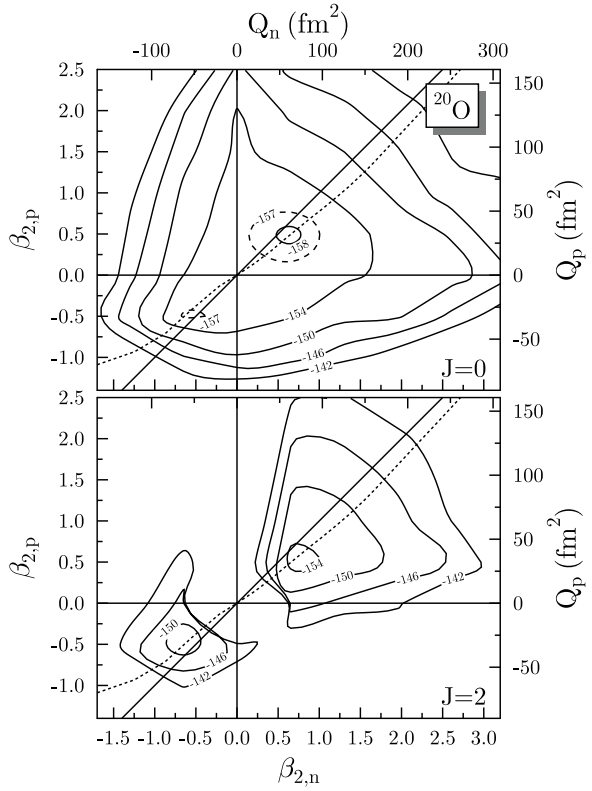

FIG. 4. Contour lines of the angular-momentum and particle-particle number projected deformation energy surface of ^{20}O (in MeV) as a function of the neutron and proton deformation $\beta_{2,q}$, $q = n, p$. The right and upper axes show the corresponding proton and neutron quadrupole moments Q_q, $q = n, p$. The upper panel shows the surface for $J = 0$, the lower panel for $J = 2$. The solid line in both panels represents the line of equal proton and neutron deformation $\beta_{2,p} = \beta_{2,n}$, the dotted line the isoscalar path followed when a single constraint on the mass quadrupole moment $\hat{Q}_t$ is applied.

already exists a decoupling of proton and neutron deformation in this only moderately neutron-rich oxygen isotope.

The 2^+ energy surface (bottom part of Fig. 4) is split into two wells in the fully prolate and oblate sectors (upper right and lower left quadrants). In the prolate sector the energy surface is markedly deeper. This gives already an indication that the collective dynamics will favor a prolate deformation of the first 2^+ state. The minimum on this surface is shifted to the region where the neutron deformation is larger than the proton deformation. This agrees with QRPA calculations [21], as well as with experimental evidence [20].

Figure 5 displays the collective GCM wave functions g^J_{kq}, Eq. (8), for the lowest $J = 0$ and $J = 2$ states obtained when restricting the collective motion to the one-dimensional path given by the dotted line in Fig. 4. On the one hand, the $J = 0$ ground-state wave function is localized in the vicinity of $\langle \hat{Q} \rangle = 0$, as expected from the potential energy surface. On the other hand, it displays an asymmetry favoring prolate deformations.

In an attempt to systematically add states that cover the whole β_n-β_p plane to the one-dimensional calculation depicted in Fig. 5, it turns out that the GCM basis becomes quickly

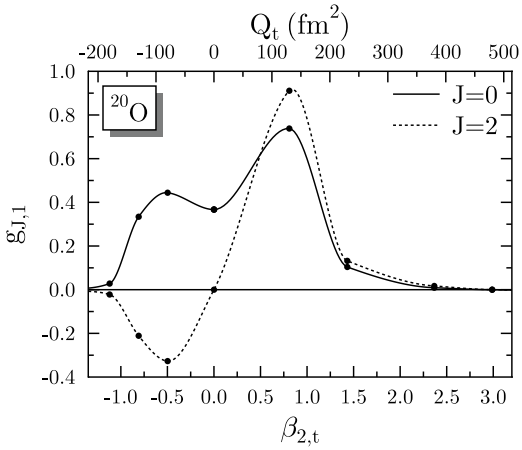

FIG. 5. GCM wave functions of the 0^+ ground state and the lowest $J = 2$ state of ^{20}O for a collective motion restricted to one dimension, plotted versus the mass quadrupole deformation $\beta_{2,t}$.

highly redundant, which is reflected by the presence of a rapidly increasing number of very small eigenvalues of the norm kernel. To avoid spurious states which would lead to large numerical inaccuracies on energies and transition probabilities, one must avoid a very dense and regular two-dimensional mesh. This problem is particularly pronounced in a light nucleus as ^{20}O, in which a SCMF wave function changes very slowly with deformation, but becomes more marginal for nuclei beyond the *sd* shell. Therefore, one has to make several calculations with different choices for the set of SCMF states, and use the variational principle to select the mesh giving the lowest energies without giving rise to spurious contributions. Starting from the one-dimensional path, we have constructed several near-equivalent sets which have a very different distribution in the $\langle\hat{Q}_n\rangle, \langle\hat{Q}_p\rangle$ plane but lead to nearly the same eigenvalues. The number of discretization points in these sets varies between 12 and 20 and must be irregularly distributed to avoid spurious eigenstates. Moreover, the number of points close to the minima in the energy surfaces has to be limited to 3 or 4.

The properties of the first 2^+ level are summarized in Table I. The uncertainty given in Table I is a measure of the fluctuations of the results when using a different set of points in the $\{\langle\hat{Q}_n\rangle, \langle\hat{Q}_p\rangle\}$ space before entering a zone of numerical instability. It is noteworthy that the $B(E2)$ value (and its equivalent for the neutron density distribution) fluctuate much more in dependence of the chosen set of SCMF states than the total energies of the first 0^+ and 2^+ states.

TABLE I. Properties of the lowest calculated 2^+ state in ^{20}O for the two choices of the deformation space considered here in comparison with experimental data taken from Ref. [1].

Deformation space	E (MeV)	$B(E2\uparrow)$ (e^2 fm^4)
$\{\langle\hat{Q}_t\rangle\}$	3.1 ± 0.1	80 ± 10
$\{\langle\hat{Q}_n\rangle, \langle\hat{Q}_p\rangle\}$	3.2 ± 0.2	180 ± 50
Experiment	1.7	28 ± 2

The energy gained from the full isospin dynamics with respect to the one-dimensional dynamics is of about 800 keV for both the ground state and the lowest 2^+ state, which leaves the excitation energy of the 2^+ state nearly unchanged. The experimental value is overestimated by 1.4 MeV. This discrepancy is in the range of values observed in a global study of the properties of the first 2^+ states in even-even nuclei [38], performed with a method similar to the one-dimensional GCM used here. The possible origins of this discrepancy are also discussed in Ref. [38], and for ^{20}O, they are presumably twofold. First, the variational calculation would be improved for the lowest 2^+ state if it was constructed from a $J_z = 2$ cranked constrained set of wave functions rather than from $J_z = 0$ set as is done here. Second, there is also a lack of broken-pair two-quasiparticle components breaking time reversal invariance in the variational space, which could play a role in this semi-magic nucleus, see the discussion of chains of heavier semi-magic nuclei in Ref. [38].

In disagreement with the global trend found by Sabbey *et al.* [38], the $B(E2)$ value is in much worse agreement with the data than the excitation energy. The effect of a larger variational space from a double constraint is even going in the wrong direction, leading to an overestimation of the $B(E2)$ value by a factor 6. The value of the ratio between neutron and proton transition matrix elements is $M_n/M_p \approx 2.1 > N/Z$. This is less than the experimental or the QRPA values calculated with the same interaction [21]. It indicates that the protons follow the neutrons too closely when deforming the nucleus, leading to the too large $B(E2)$ value that we obtain. Since the QRPA value for the $B(E2)$ obtained with the same force is much lower, this probably points to a deficiency of our variational space rather than to a particular problem due to the effective interaction. The presence of broken-pair two-quasiparticle states breaking time-reversal invariance in the 2^+ wave function could reduce the $B(E2)$ value and go into the right direction, but the present stage of our method does not allow to test the magnitude of this effect.

The representation of the two-dimensional collective wave function is complicated by the fact that the discretized GCM wave function, Eq. (3), is defined without a volume element. As a consequence, the value of the collective wave function g^J_{kq} at a given point q represents the wave function times an unspecified volume element, that depends on the distribution of the surrounding points. On the one hand, this definition of the GCM wave function allows us to optimize the set of basis states and to remove redundant states without any difficulty. On the other hand, any attempt to plot a GCM wave function built from unevenly distributed points might be very misleading as any surface used to interpolate these points to guide the eye is, strictly speaking, meaningless. A plot of a one-dimensional wave function g^J_{kq}, as given in Fig. 5, is of course also affected, but in one dimension one can almost always achieve a distribution of basis states that still allows an intuitive interpretation. There are further issues, as the only proper metric is defined by the overlap kernels, not the generator coordinates, which furthermore are different for each angular momentum. These problems, which affect the presentation and interpretation of a GCM wave function, but not its physical content, deserve further attention in the

future. However, from all the sets of points that we have used, one can conclude that the dominant contribution to the lowest $J = 0$ and $J = 2$ GCM states is a state located on the one-dimensional path with $\beta_2 \approx 0.8$.

IV. CONCLUSIONS

We have started an investigation of the large-amplitude quadrupole dynamics in neutron-rich nuclei taking into account the full isospin space. Among our initial motivation was the search for configurations in which neutron and proton display different static deformation. Our results indicate that it is indeed the case when the usual dimensionless deformations $\beta_{2,n}$ and $\beta_{2,p}$ are used to remove the trivial scaling of the quadrupole moments with neutron and proton number.

We have also looked for signs of a dynamical isospin polarization which would show up in specific spectroscopic properties. At a qualitative level, we observe the importance of allowing independent proton and neutron deformation: although the main features of the collective wave functions are still the same as those determined by the one-dimensional dynamics, the full wave function displays a significant extension on both sides of this path. Similarly, there is a clear influence on the transition moments. Unfortunately, the agreement with the experimental data is not satisfactory for this light nucleus. Our model would probably be improved by enlarging the variational space for the 2^+ state with the inclusion of states breaking time-reversal invariance. The developments which will allow this inclusion are still underway.

ACKNOWLEDGMENTS

Work by M.B. was partly performed within the framework of the Espace de Structure Nucléaire Théorique (ESNT). This work has been partly supported by the PAI P5-07 of the Belgian Science Policy Office.

[1] S. Raman, C. H. Malarkey, W. T. Milner, C. W. Nestor, Jr., and P. H. Stelson, At. Data Nucl. Data Tables **36**, 1 (1987).
[2] J. L. Escudié, R. Lombard, M. Pignanelli, F. Resmini, and A. Tarrats, Phys. Rev. C **10**, 1645 (1974); **11**, 639(E) (1975).
[3] O. Tarasov, R. Allatt, J. C. Anglique, R. Anne, C. Borcea, Z. Dlouhy, C. Donzaud, S. Grévy, D. Guillemaud-Mueller, M. Lewitowicz, S. Lukyanov, A. C. Mueller, F. Nowacki, Yu. Oganessian, N. A. Orr, A. N. Ostrowski, R. D. Page, Yu. Penionzhkevich, F. Pougheon, A. Reed, M. G. Saint-Laurent, W. Schwab, E. Sokol, O. Sorlin, W. Trinder, and J. S. Winfield, Phys. Lett. **B409**, 64 (1997).
[4] H. Sakurai, S. M. Lukyanov, M. Notani, N. Aoi, D. Beaumel, N. Fukuda, M. Hirai, E. Ideguchi, N. Imai, M. Ishihara, H. Iwasaki, T. Kubo, K. Kusaka, H. Kumagai, T. Nakamura, H. Ogawa, Yu. E. Penionzhkevich, T. Teranishi, Y. X. Watanabe, K. Yoneda, and A. Yoshida, Phys. Lett. **B448**, 180 (1999).
[5] A. Ozawa, O. Bochkarev, L. Chulkov, D. Cortina, H. Geissel, M. Hellström, M. Ivanov, R. Janik, K. Kimura, T. Kobayashi, A. A. Korsheninnikov, G. Münzenberg, F. Nickel, A. A. Ogloblin, M. Pfützner, V. Pribora, H. Simon, B. Sitárd, P. Strmen, K. Sümmerer, T. Suzuki, I. Tanihata, M. Winkler, and K. Yoshida, Nucl. Phys. **A673**, 411 (2000).
[6] M. Thoennessen, T. Baumann, J. Enders, N. H. Frank, P. Heckman, J. P. Seitz, A. Stolz, and E. Tryggestad, Nucl. Phys. **A722**, 61c (2003).
[7] M. Thoennessen, T. Baumann, B. A. Brown, J. Enders, N. Frank, P. G. Hansen, P. Heckman, B. A. Luther, J. Seitz, A. Stolz, and E. Tryggestad, Phys. Rev. C **68**, 044318 (2003).
[8] M. Belleguic, M.-J. Lòpez-Jiménez, M. Stanoiu, F. Azaiez, M.-G. Saint-Laurent, O. Sorlin, N. L. Achouri, J.-C. Angélique, C. Bourgeois, C. Borcea, J.-M. Daugas, C. Donzaud, F. De Oliveira-Santos, J. Duprat, S. Grévy, D. Guillemaud-Mueller, S. Leenhardt, M. Lewitowicz, Yu.-E. Penionzhkevich, and Yu. Sobolev, Nucl. Phys. **A682**, 136c (2001).
[9] Y. Blumenfeld, Nucl. Phys. **A752**, 279c (2005).
[10] J. K. Jewel, L. A. Riley, P. D. Cottle, K. W. Kemper, T. Glasmacher, R. W. Ibbotson, H. Scheit, M. Chromik, Y. Blumenfeld, S. E. Hirzebruch, F. Maréchal, and T. Suomijärvi, Phys. Lett. **B454**, 181 (1999).
[11] P. G. Thirolf, B. V. Pritychenko, B. A. Brown, P. D. Cottle, M. Chromik, T. Glasmacher, G. Hackman, R. W. Ibbotson, K. W. Kemper, T. Otsuka, L. A. Riley, and H. Scheit, Phys. Lett. **B485**, 16 (2000).
[12] M. Stanoiu, F. Azaiez, Zs. Dombrádi, O. Sorlin, B. A. Brown, M. Belleguic, D. Sohler, M. G. Saint Laurent, J. Lopez-Jimenez, Y. E. Penionzhkevich, G. Sletten, N. L. Achouri, J. C. Angélique, F. Becker, C. Borcea, C. Bourgeois, A. Bracco, J. M. Daugas, Z. Dlouhý, C. Donzaud, J. Duprat, Zs. Fülöp, D. Guillemaud-Mueller, S. Grévy, F. Ibrahim, A. Kerek, A. Krasznahorkay, M. Lewitowicz, S. Leenhardt, S. Lukyanov, P. Mayet, S. Mandal, H. van der Marel, W. Mittig, J. Mrázek, F. Negoita, F. De Oliveira-Santos, Zs. Podolyák, F. Pougheon, M. G. Porquet, P. Roussel-Chomaz, H. Savajols, Y. Sobolev, C. Stodel, J. Timár, and A. Yamamoto, Phys. Rev. C **69**, 034312 (2004).
[13] E. Becheva, Y. Blumenfeld, E. Khan, D. Beaumel, J. M. Daugas, F. Delaunay, Ch-E. Demonchy, A. Drouart, M. Fallot, A. Gillibert, L. Giot, M. Grasso, N. Keeley, K. W. Kemper, D. T. Khoa, V. Lapoux, V. Lima, A. Musumarra, L. Nalpas, E. C. Pollacco, O. Roig, P. Roussel-Chomaz, J. E. Sauvestre, J. A. Scarpaci, F. Skaza, and H. S. Than, Phys. Rev. Lett. **96**, 012501 (2006).
[14] T. Aumann, Nucl. Phys. **A752**, 289c (2005).
[15] E. Sauvan, F. Carstoiu, N. A. Orr, J. S. Winfield, M. Freer, J. C. Angélique, W. N. Catford, N. M. Clarke, N. Curtis, S. Grévy, C. Le Brun, M. Lewitowicz, E. Liégard, F. M. Marqués, M. Mac Cormick, P. Roussel-Chomaz, M.-G. Saint Laurent, and M. Shawcross, Phys. Rev. C **69**, 044603 (2004).
[16] R. Palit, P. Adrich, T. Aumann, K. Boretzky, D. Cortina, U. Datta Pramanik, Th.W. Elze, H. Emling, M. Fallot, H. Geissel, M. Hellström, K. L. Jones, L. H. Khiem, J. V. Kratz, R. Kulessa, Y. Leifels, A. Leistenschneider, G. Münzenberg, C. Nociforo, P. Reiter, H. Simon, K. Sümmerer, and W. Walus, Nucl. Phys. **A731**, 235 (2004).
[17] D. Cortina-Gil, J. Fernandez-Vazquez, T. Aumann, T. Baumann, J. Benlliure, M. J. G. Borge, L. V. Chulkov, U. Datta Pramanik, C. Forssén, L. M. Fraile, H. Geissel, J. Gerl, F. Hammache, K. Itahashi, R. Janik, B. Jonson, S. Mandal, K. Markenroth, M. Meister, M. Mocko, G. Münzenberg, T. Ohtsubo, A. Ozawa, Y. Prezado, V. Pribora, K. Riisager, H. Scheit, R. Schneider,

G. Schrieder, H. Simon, B. Sitar, A. Stolz, P. Strmen, K. Sümmerer, I. Szarka, and H. Weick, Phys. Rev. Lett. **93**, 062501 (2004).
[18] M. Stanoiu, F. Azaiez, Zs. Dombrádi, O. Sorlin, B. A. Brown, M. Belleguic, D. Sohler, M. G. Saint Laurent, Y. E. Penionzhkevich, G. Sletten, C. Borcea, C. Bourgeois, A. Bracco, J. M. Daugasd, Z. Dlouhý, C. Donzaud, Zs. Fülöp, D. Guillemaud-Mueller, S. Grévy, F. Ibrahim, A. Kerek, A. Krasznahorkay, M. Lewitowicz, S. Lukyanov, P. Mayet, S. Mandal, W. Mittig, J. Mrázeki, F. Negoita, F. De Oliveira-Santos, Zs. Podolyák, F. Pougheon, P. Roussel-Chomaz, H. Savajols, Y. Sobolev, C. Stodel, J. Timár, and A. Yamamoto, Nucl. Phys. **A746**, 135c (2004).
[19] E. Khan and Nguyen Van Giai, Phys. Lett. **B472**, 253 (2000).
[20] E. Khan, Y. Blumenfeld, Nguyen Van Giai, T. Suomijärvi, N. Alamanos, F. Auger, G. Colò, N. Frascaria, A. Gillibert, T. Glasmacher, M. Godwin, K. W. Kemper, V. Lapoux, I. Lhenry, F. Maréchal, D. J. Morrissey, A. Musumarra, N. A. Orr, S. Ottini-Hustache, P. Piattelli, E. C. Pollacco, P. Roussel-Chomaz, J. C. Roynette, D. Santonocito, J. E. Sauvestre, J. A. Scarpaci, and C. Volpe, Phys. Lett. **B490**, 45 (2000).
[21] E. Khan, N. Sandulescu, M. Grasso, and Nguyen Van Giai, Phys. Rev. C **66**, 024309 (2002).
[22] G. Giambrone, S. Scheit, F. Barranco, P. F. Bortignon, G. Colò, D. Sarchi, and E. Vigezzi, Nucl. Phys. **A726**, 3 (2003).
[23] A. Obertelli, S. Péru, J.-P. Delaroche, A. Gillibert, M. Girod, and H. Goutte, Phys. Rev. C **71**, 024304 (2005).
[24] D. Vretenar, A. V. Afanasjev, G. A. Lalazissis, and P. Ring, Phys. Rep. **409**, 101 (2005).
[25] Y. Utsuno, T. Otsuka, T. Mizusaki, and M. Honma, Phys. Rev. C **60**, 054315 (1999).
[26] B. A. Brown, P. G. Hansen, and J. A. Tostevin, Phys. Rev. Lett. **90**, 159201 (2003).
[27] A. Volya and V. Zelevinsky, Phys. Rev. Lett. **94**, 052501 (2005).
[28] A. Valor, P.-H. Heenen, and P. Bonche, Nucl. Phys. **A671**, 145 (2000).
[29] M. Bender, P. Bonche, T. Duguet, and P.-H. Heenen, Phys. Rev. C **69**, 064303 (2004).
[30] M. Bender and P.-H. Heenen, Eur. Phys. J. A **25**, 519 (2005).
[31] B. Gall, P. Bonche, J. Dobaczewski, H. Flocard, and P.-H. Heenen, Z. Phys. A **348**, 183 (1994).
[32] J. Terasaki, P.-H. Heenen, H. Flocard, and P. Bonche, Nucl. Phys. **A600**, 271 (1996).
[33] E. Chabanat, P. Bonche, P. Haensel, J. Meyer, and R. Schaeffer, Nucl. Phys. **A635**, 231 (1998); Nucl. Phys. **A643**, 441(E) (1998).
[34] M. Bender, H. Flocard, and P.-H. Heenen, Phys. Rev. C **68**, 044321 (2003).
[35] M. Bender and P.-H. Heenen, Nucl. Phys. **A713**, 39 (2003).
[36] K. Rutz, J. A. Maruhn, P.-G. Reinhard, and W. Greiner, Nucl. Phys. **A590**, 680 (1995).
[37] P. Bonche, J. Dobaczewski, H. Flocard, P.-H. Heenen, and J. Meyer, Nucl. Phys. **A510**, 466 (1990).
[38] B. Sabbey, M. Bender, G. Bertsch, and P.-H. Heenen, Phys. Rev. C **75**, 044305 (2007).